Geochemistry, Geophysics, Geosystems®

AGU ADVANCING EARTH AND SPACE SCIENCES

RESEARCH ARTICLE
10.1029/2025GC012803

Late Holocene Increase in Influence of Pacific Deep Water off Southern Chile Caused by Migration of the Southern Westerly Wind: Evidence From Beryllium Isotopes

Karin Nemoto[1,2], Yusuke Yokoyama[1,2,3,4], Adam David Sproson[5], Yosuke Miyairi[1], Takahiro Aze[1], Yair Rosenthal[6], Samantha Bova[7], and Hailey Riechelson[6]

[1]Atmosphere and Ocean Research Institute, The University of Tokyo, Kashiwa, Japan, [2]Department of Earth and Planetary Science, The University of Tokyo, Kashiwa, Japan, [3]Graduate Program on Environmental Studies, The University of Tokyo, Kashiwa, Japan, [4]Research School of Physics, The Australian National University, Canberra, ACT, Australia, [5]National Oceanography Centre, Southampton, UK, [6]Department of Marine Science, Rutgers University, New Brunswick, NJ, USA, [7]Department of Geological Sciences, San Diego State University, San Diego, CA, USA

Abstract The Southern Hemisphere westerly winds and the Antarctic Circumpolar Current, both located offshore Chile, are key components of global climate due to their influence on Southern Ocean upwelling and nutrient utilization with implications for atmospheric CO_2. In this study, the Holocene upwelling history of the Chilean continental margin is reconstructed using beryllium isotopes in the reactive phase of marine sediments collected off the coast of southern Chile. The increase in $^{10}Be/^{9}Be$ throughout the Holocene reflects the strengthening of coastal upwelling due to the southward shift of the Southern Hemisphere westerly winds, which is consistent with increased productivity along the Chilean margin. These observed changes support the idea that complete utilization of nitrate, exported from the Southern Ocean, likely acted to reduce the Southern Ocean's contribution to the increase in atmospheric CO_2 during the Holocene.

Plain Language Summary It was proposed that upwelled carbon rich deep water coupled with nutrient utilization along the Chilean margin reduced the contribution of the Southern Ocean as a major source of CO_2 to the atmosphere during the Holocene (11,700 years ago to present). However, Holocene upwelling history along the Chilean margin has not yet been directly reconstructed. We have measured reactive phase beryllium isotopes in a marine sediment core recovered from offshore Chile to trace the strength of upwelling during the Holocene. Today, beryllium isotopes along the Chilean margin are controlled by the mixing of beryllium sourced from land and ocean waters. We found that the mixing between these sources also controlled beryllium isotopes during the Holocene. The results suggest an increase in productivity and decrease in terrigenous input offshore Chile, which indicates that upwelling increased along the central Chilean margin during the Holocene. This view is consistent with the hypothesis that carbon sequestration to the ocean driven by Chilean margin upwelling and associated nutrient consumption reduced the contribution of the Southern Ocean CO_2 release to the atmosphere from the ocean during the Holocene.

Key Points:

- Reactive beryllium isotopes are used as new proxy for upwelling along the Chilean margin during the Holocene
- Enhanced upwelling during the Holocene along the Chilean margin is directly reconstructed for the first time
- Complete utilization of nutrients along the Chilean margin reduced carbon dioxide emission to the atmosphere during the Holocene

Supporting Information:

Supporting Information may be found in the online version of this article.

Correspondence to:

K. Nemoto and Y. Yokoyama,
nemoto@aori.u-tokyo.ac.jp;
yokoyama@aori.u-tokyo.ac.jp

Citation:

Nemoto, K., Yokoyama, Y., Sproson, A. D., Miyairi, Y., Aze, T., Rosenthal, Y., et al. (2026). Late Holocene increase in influence of Pacific deep water off Southern Chile caused by migration of the Southern Westerly Wind: Evidence from beryllium isotopes. *Geochemistry, Geophysics, Geosystems*, *27*, e2025GC012803. https://doi.org/10.1029/2025GC012803

Received 21 NOV 2025
Accepted 30 JAN 2026

Author Contributions:

Conceptualization: Yusuke Yokoyama, Adam David Sproson, Yair Rosenthal, Samantha Bova
Data curation: Yusuke Yokoyama, Yosuke Miyairi, Takahiro Aze
Formal analysis: Yosuke Miyairi, Takahiro Aze, Yair Rosenthal, Hailey Riechelson
Funding acquisition: Yusuke Yokoyama, Adam David Sproson, Yair Rosenthal, Samantha Bova

1. Introduction

The Southern Westerly Wind (SWW) belt plays a major role in the global climate. This wind jet, currently positioned in central Chile (40°S–60°S), controls the position and the strength of the Antarctic Circumpolar Current (ACC; Figure 1), thereby exerting an important influence on ocean-atmosphere heat and carbon dioxide (CO_2) exchange in the Southern Ocean on seasonal and longer time scales (Anderson et al., 2009; Fyfe & Saenko, 2006; Lovenduski et al., 2008). At present, the strength and position of the SWW vary seasonally, extending northward into central Chile (33°–40°S) during austral winters and south Chile (50°–55°S) during austral summers. When the SWW and the ACC move southward, more surface water is deflected northward, enhancing upwelling in the Southern Ocean. The upwelled carbon rich deep water coupled with inefficient nutrient utilization at the surface is a major source of CO_2 to the atmosphere (Menviel & Spence, 2024; Saunders et al., 2018; Toggweiler et al., 2006). Indeed, the increase in atmospheric CO_2 concentration during the last deglaciation has been attributed to this atmosphere-ocean coupling (Anderson et al., 2009; Gray et al., 2023; Siani et al., 2013).

In the eastern Pacific Ocean, the SWW and the ACC are presently positioned in southern Chile offshore the Patagonian Ice Sheet (PIS). Here the position of the SWW exerts the dominant control on precipitation, making it

Investigation: Yusuke Yokoyama, Adam David Sproson, Yair Rosenthal, Samantha Bova, Hailey Riechelson
Methodology: Yusuke Yokoyama, Adam David Sproson, Yosuke Miyairi, Takahiro Aze, Yair Rosenthal
Project administration: Yair Rosenthal, Samantha Bova
Resources: Yusuke Yokoyama
Supervision: Yusuke Yokoyama
Writing – review & editing: Yusuke Yokoyama, Adam David Sproson, Yosuke Miyairi, Takahiro Aze, Yair Rosenthal, Samantha Bova, Hailey Riechelson

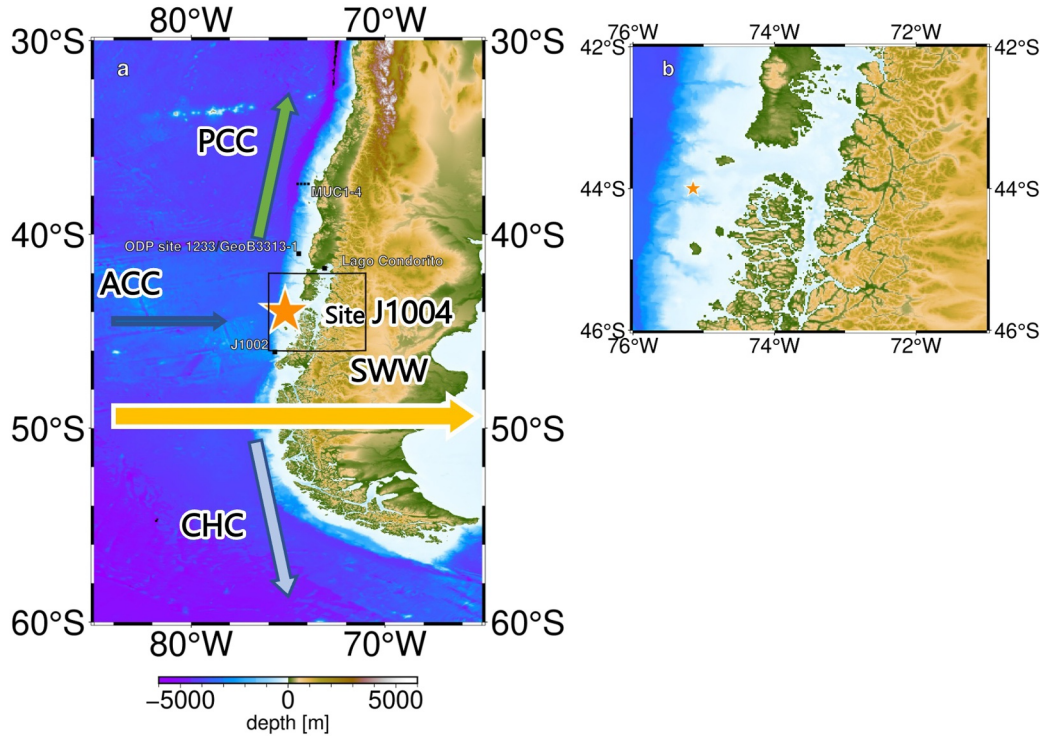

Figure 1. (a) Map of South America and East South Pacific displaying site J1004A (the orange star) in relation to previous sampling sites (black squares) with major sea currents. Antarctic Circumpolar Current (ACC; dark blue arrow), Peru-Chile Current (PCC; green arrow) and Cape-Horn Current (CHC; sky blue arrow) are shown. Site J1004 is in the northern edge of the SWWs (yellow arrow). The area inside the black rectangle box is enlarged in (b).

an ideal location to reconstruct the position and/or strength of the SWW by tracing the delivery of sediments from land to the continental margin on the western side of Chile (Lamy et al., 2010). Using this approach, previous studies have shown that the SWW shifted equatorward during the Last Glacial Maximum (LGM) relative to a more poleward position during the Holocene (McGlone et al., 2019; Moreno et al., 2021; Saunders et al., 2018). During the Holocene, reconstruction suggests that the SWW was relatively weak before ~8 ka, in both the western and eastern sectors of the Pacific (McGlone et al., 2019; Moreno et al., 2021; Riechelson et al., 2023).

SWW shifts also affect productivity in the south Pacific. When the SWW migrate south, upwelling and nutrient delivery to the Southern Ocean increase, which results in less complete nitrogen utilization and less efficient biological pumping (Studer et al., 2018). The unutilized nutrient is advected downstream to regions such as the Chilean margin and may reach as far as the Western Pacific Warm Pool and Eastern Equatorial Pacific. Riechelson et al. (2024) suggested that productivity in those regions was enhanced during the Holocene because of enhanced nutrient delivery driven by a southward migration of the SWW. However, the hypothesized increase in upwelling during the Holocene is not directly validated by their data. To test this hypothesis, we use records of beryllium isotopes and X-ray fluorescence (XRF) from the continental shelf off the coast of Chile covering the Holocene to trace upwelling associated with variations in the strength and/or position of the SWW and the ACC.

2. Beryllium Isotopes as Proxies of Upwelling

We have measured reactive phase Be isotopes (Yokoyama & Sproson, 2026) in a marine sediment core J1004A located offshore Chile (44.0005°S, 75.1511°W; Figure 1). The cosmogenic radionuclide ^{10}Be ($T_{1/2}$ = 1.39 Myr) (Chmeleff et al., 2010) is produced by the interaction of cosmic rays with oxygen and nitrogen in the atmosphere (meteoric production) and deposited onto the Earth's surface via precipitation or dust (Lal, 1991). The stable isotope ^{9}Be is present in silicate rocks and is released into rivers during chemical weathering. A certain fraction of ^{10}Be and ^{9}Be atoms released into the Earth's surface adsorbs onto mineral surfaces or co-precipitates with iron and manganese oxyhydroxides. This Be pool, which is often referred to as the reactive phase, exchanges with dissolved Be through dissolution–precipitation or desorption–adsorption reactions. The ^{10}Be/^{9}Be of both the reactive

and dissolved phases rapidly reach equilibrium and are therefore identical (von Blanckenburg et al., 2012). An advantage of using the ratio of ^{10}Be to ^{9}Be (^{10}Be/^{9}Be) is the removal of secondary effects such as grain size and dilution effects (Wittmann et al., 2012).

The ^{10}Be/^{9}Be ratio has various applications. In previous studies, the ^{10}Be/^{9}Be ratio has been used to reconstruct the Antarctic Ice Sheet related processes (Yokoyama & Sproson, 2026). As a result of ^{10}Be deposition from the atmosphere to the ice sheet for a long time, ice sheet melt water has a relatively high ^{10}Be/^{9}Be ratio and therefore it was proposed that ^{10}Be/^{9}Be was a proxy for ice sheet meltwater flux (Behrens et al., 2019, 2022; Sproson, Takano, et al., 2021, 2022). Similarly, the relative proximity of fluvial inputs from the Patagonian Ice Sheet primarily characterized the ^{10}Be/^{9}Be ratio of Chilean margin sediments during the last glacial period (Sproson et al., 2024). The latter finding is based on observations by Wittmann et al. (2017) who found that the ^{10}Be/^{9}Be ratio of the reactive phase in a shelf transect of surface sediments (MUC1-4) reflects variability in the mixing of fluvial and seawater sources on the Chilean margin. Beryllium-10 is enriched in seawater because of the large aerial input from the atmosphere to the ocean surface in contrast to ^{9}Be, which is enriched in fluvial material from the chemical weathering of rocks. Furthermore, based on ^{10}Be/^{9}Be values of surface sediments around the Antarctic, Jeromson et al. (2024, 2025) initially proposed that Be isotopes may be used as an upwelling proxy.

Therefore, three possible mechanisms can account for downcore variations in beryllium isotopes: (a) a change in the Be isotope composition of the marine end-member, linked to fluctuations in global ^{10}Be production rates and/or the water mass accessing Site J1004; (b) a shift in the local weathering regime which modifies the terrestrial end-member; and (c) a change in the relative proportion of marine and terrestrial signatures linked to sediment supply, global mean sea level, the proximity of the PIS to the continental shelf edge, and/or ocean mixing. A previous study found that mechanism (a) did not have a significant effect during the past 130 ky, but mechanism (b) and (c) dominated reactive Be isotopes during the deglaciation period when the PIS retreated from the continental shelf edge to its modern configuration (Sproson et al., 2024). During the Holocene, however, the PIS was already close to its present position and the ice sheet processes described above may have no longer contributed to ^{10}Be/^{9}Be on the Chilean margin. Instead, fluvial changes have been dominated by changes in precipitation, which are linked to shifts in the location of the SWW (Riechelson et al., 2023). To date, no studies have discussed ^{10}Be/^{9}Be ratio changes on the Chilean margin during the Holocene when PIS was relatively stable compared with the deglaciation period. When the influence of sea level change and icesheet fluctuations on mechanism (c) is small, the dominant mechanism affecting ^{10}Be/^{9}Be is likely a change in the oceanic contribution to the site.

3. Regional Setting

Offshore mid-latitude Chile at ~45°S, the ACC splits into the Peru-Chile Current (PCC), flowing northward, and the Cape-Horn Current, flowing southward (Figure 1). Site J1004, discussed here, located close to the modern bifurcation region between the two surface currents, is sensitive to migrations of the SWW (Figure 1). The ACC brings relatively cold subantarctic water to offshore Chile, causing steep latitudinal temperature gradients off the coast of Chile. Westerly winds ascend along the western side of the Andes, causing high rates of precipitation (>2,000 mm/yr), as supported by the strong correlation between precipitation and wind strength (Garreaud et al., 2013). At Site J1004, precipitation increases during austral winter, when the SWWs migrate north, increasing the influence of fresh continental runoff near the site. Bottom water at this site is under the influence of the upper Pacific Deep Water.

4. Material and Methods

4.1. Core Description

Site J1004 was located 60 km offshore Aysén Region of Chile (44.0005°S, 75.1511°W) at 1,125 m water depth, and the coring was performed during Expedition 379T aboard the D/V JOIDES Resolution in August 2019 (Figure 1; Bova et al., 2019). The collected core length reached 60.94 m below sea floor. The sediment core is assigned to two lithologic units. Unit I (upper 58 mbsf) is composed of nannofossil-bearing diatom rich clay and ash-bearing clay and silty clay (Figure S1 in Supporting Information S1). Unit I can be divided into two lithological subunits, a nannofossil-bearing diatom rich clay (0–51 mbsf) and diatom bearing silty clay (51–58 mbsf). Unit II was assigned to sediment below 58 mbsf composed of large (5–10 cm-sized) gravel clasts. The age model

for J1004 published by Riechelson et al. (2023) reveals a relatively constant sedimentation rate of ~6 m/kyr for the entire record, which spans from 85 years BP to ~11,300 years BP.

4.2. Beryllium Isotopes Analysis

Reactive phase Be isotopes, ^{10}Be and ^{9}Be, measurements were performed on 37 samples from site J1004 hole A and provide 200–300 years resolution following the age model of Riechelson et al. (2023). Be isotopes in sediments were measured following the methods of Bourles et al. (1989) and Sproson, Takano, et al. (2021). The reactive phase of marine sediments was leached using a 20 mL/g sediment of 0.04 M hydroxylamine hydrochloride solution in 25% acetic acid at 80°C for 6 hr. A 2 mL aliquot was taken for ^{9}Be measurement. The remaining solution was spiked with 3 ml of a 0.101 mg/ml ^{9}Be carrier to determine ^{10}Be concentrations of samples from the measured beryllium isotope ratios. Beryllium was purified using two solvent extractions of acetylacetone in the presence of EDTA (Bourles et al., 1989; Sproson, Takano, et al., 2021), followed by the precipitation of $Be(OH)_2$ with NH_4 (Kohl & Nishiizumi, 1992). The resulting hydroxide was dried in a quartz vial and converted to BeO using a microwave ceramic crucible for 5 min (Yokoyama et al., 2019). The BeO powder was mixed with niobium (Nb) powder and inserted into a copper cathode for the measurement of reactive ^{10}Be abundance using an AMS (Yokoyama et al., 2019).

Beryllium-10 and Beryllium-9 ratios were measured using a National Electrostatic Corporation (NEC) accelerator mass spectrometer (AMS), of 5 MV terminal voltage, at the University of Tokyo, Micro Analysis Laboratory, Tandem accelerator (MALT; Matsuzaki et al., 2007). Absolute values were obtained using the KNB5-2 standard (^{10}Be/^{9}Be = 8.558 × 10^{-12}; Nishiizumi et al., 2007) with a typical beam current of 2–5 μA (^{9}Be^{16}O−). Decay correction is performed on $[^{10}Be]_{reactive}$ cells using a ^{10}Be half-life of 1.387 Ma (Chmeleff et al., 2010). The concentration of ^{9}Be was measured using a Thermo® ELEMENT XR high-resolution inductively coupled plasma mass spectrometer (HR-ICP-MS) at the Atmosphere and Ocean Research Institute (AORI), UTokyo (Sproson, Aze, et al., 2021). The ^{10}Be/^{9}Be ratios were corrected for ^{10}Be paleo-production using the paleomagnetic reference records of the geomagnetic dipole moment (Korte et al., 2011) following von Blanckenburg et al. (2015).

4.3. Isotope Analysis for Foraminifera

Planktonic and benthic foraminifera (*N. pachyderma* and *U. peregrina*, respectively) were picked from the >125 μm size fraction and sonicated in MilliQ water to remove debris prior to analyzing δ^{18}O on a Micromass Optima mass spectrometer with a Multiprep device at Rutgers University. The long-term precision for δ^{18}O is ±0.08‰ (2σ).

5. Results

Given the dramatic shift in lithology between Units I and II discussed above (Figure S1 in Supporting Information S1), our climate interpretations here are restricted to the 0–57 mbsf of the core (Unit I) shown in Figures 2 and 3. Results of the complete records are shown in Figures S2 and S3 of Supporting Information S1. The $[^{9}Be]_{reactive}$, $[^{10}Be]_{reactive}$ and ^{10}Be/^{9}Be ranges from 0.90 to 1.73 × 10^{16} (Figure 2a), 3.35 to 5.90 × 10^{8} (Figure 2b) and 2.65 to 6.05 × 10^{-8} (Figure 2c), respectively. The average ^{10}Be/^{9}Be ratio is 1.5 × 10^{-8} at the bottom of the record, dated to 9.4 ka. The average ^{10}Be/^{9}Be ratio then gradually increases to ~3.5 × 10^{-8} in the Mid Holocene (8.2–4.2 ka) and ~5.5 during the Late Holocene (4.2 ka to present) close to the modern continental shelf ^{10}Be/^{9}Be ratio (Figure S4 in Supporting Information S1). The total organic carbon (TOC) shows similar trends to ^{10}Be/^{9}Be (Figure 2d). TOC contents increased to 2.36% in the Mid Holocene from 1.88% in the Late Holocene. On average, the δ^{18}O of planktonic and benthic foraminifera (*N. pachyderma* and *U. peregrina*) shifted toward heavier values from the early to late Holocene, likely reflecting cooling of the water (Figures 2e–2g).

6. Discussion

The observed long-term decrease of terrigenous elements (Al, Ca, Si, Ti, Fe, K, and Zr) over the Holocene, measured by XRF core scanning, at this site, is attributable to a southward shift of the SWW (Riechelson et al., 2023). Concomitant with the long-term decrease in the terrigenous flux, there is an increase in TOC mass accumulation across the Holocene, reflecting an increase in productivity (Riechelson et al., 2023). As demonstrated in the following sections, the Be data show that the increase in biological productivity reflects changes in

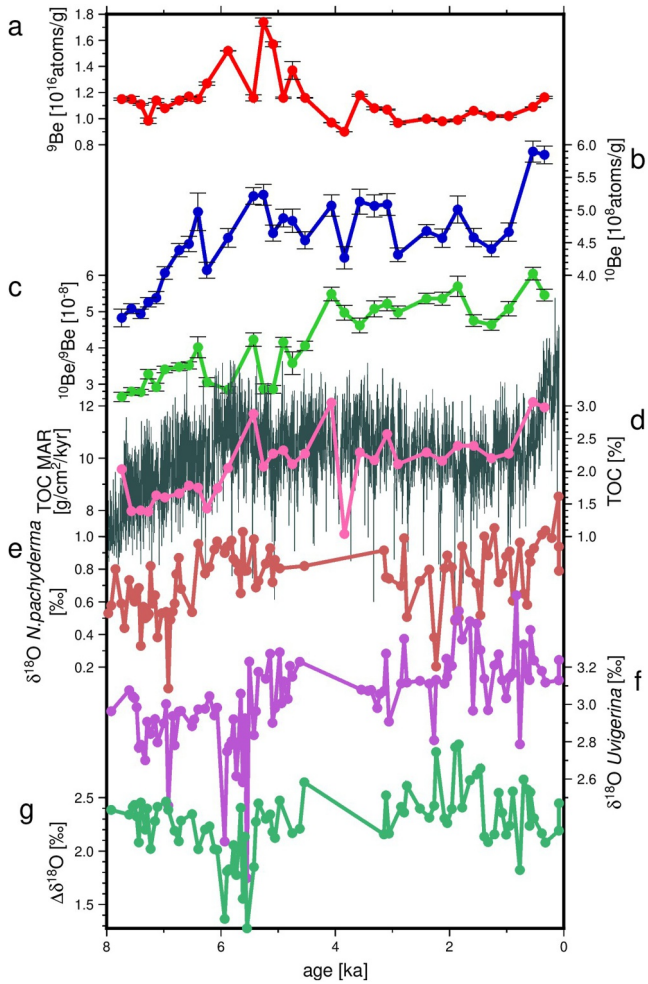

Figure 2. Results for geochemical analysis on Core J1004A. (a) Concentration of reactive ^{9}Be and (b) ^{10}Be. (c) Reactive ^{10}Be/^{9}Be ratio. (d) Total organic carbon content (this study; pink) and its mass accumulation rate (Riechelson et al., 2024; green). δ^{18}O of (e) planktonic foraminifera *N. pachyderma*, (f) benthic foraminifera *U. peregrina*, and (g) δ^{18}O difference between planktonic foraminifera *N. pachyderma* and benthic foraminifera *U. peregrina*.

nutrient supply to the Chilean Margin driven by enhanced upwelling and intrusion of Pacific Deep Water (PDW) along the margin and within the ACC across the Holocene.

6.1. Declining Terrestrial Freshwater Inputs Throughout the Holocene

With respect to the relative $[^{10}Be]_{reactive}$ versus $[^9Be]_{reactive}$ relationship presented in Figure 3, a 1:1 linear regression would suggest that a similar fluctuation in both isotopes is controlled by the concentration effect (von Blanckenburg et al., 2015). However, here we find the slope is positive with its gradient less than 1, suggesting additional variability related to changes in $[^{10}Be]_{reactive}$ inputs (von Blanckenburg et al., 2015), which largely control variations in ^{10}Be/^{9}Be (Figure 3). This resembles the relationship recorded for Site J1002 over the last glacial cycle (Sproson et al., 2024) and surface sediments from a transect across the northern Chilean margin Wittmann et al. (2017), suggesting that the variations in ^{10}Be/^{9}Be recorded here reflect the relative contribution of ^{10}Be from fluvial and marine sources. Possible causes for this change in ^{10}Be/^{9}Be ratios are: (a) a decrease in freshwater supply (low ^{10}Be/^{9}Be) from the Andes via precipitation; (b) variable erosional fluxes (low ^{10}Be/^{9}Be) due to glacial/interglacial advance/retreat of the PIS or rainfall during the Holocene; and (c) changes in the contribution of deep Pacific water containing a higher ^{10}Be/^{9}Be concentrations than freshwater (Kusakabe et al., 1990). In this study, ice sheet related processes, as proposed by previous studies (Behrens et al., 2019, 2022; Sproson et al., 2022, 2024; White et al., 2019; Yokoyama, Anderson, et al., 2016), are not considered as playing an important role in characterizing ^{10}Be/^{9}Be at Site J1004 because the PIS around this site had already retreated to modern configurations before the Holocene (Davies et al., 2020). In the following section, we discuss the cause of the ^{10}Be/^{9}Be increase throughout the Holocene at Site J1004.

A decrease in precipitation and freshwater supply from the Andes is a potential cause of the increased ^{10}Be/^{9}Be ratio. However, precipitation records based on pollen assemblage do not correspond to ^{10}Be/^{9}Be records at Site J1004, implying a minor role of precipitation in determining ^{10}Be/^{9}Be at Site J1004 (Moreno et al., 2010, 2021; Figure 4b). Variable rates of erosion from the PIS (low ^{10}Be/^{9}Be) have been implicated in changing the ^{10}Be/^{9}Be at a nearby sites during the last deglaciation (Sproson et al., 2024). Terrigenous inputs to the core site from glacial erosion deliver ^{10}Be/^{9}Be that is significantly lower than seawater as observed previously in Antarctica (Behrens et al., 2019, 2022; Jeromson et al., 2024; Sproson et al., 2021a, 2022; Yokoyama, Maeda, et al., 2016) and the Chilean margin Sproson et al. (2024). Thus, relatively less input of terrigenous material from the PIS is a potential cause of the increase of ^{10}Be/^{9}Be at Site J1004. Most of the icesheet around 44°S, however, had retreated by ~11 ka according to a recent reconstruction of the PIS (Davies et al., 2020) and therefore did not likely impact sedimentation at the site substantially, as evident in the stable sedimentation rate since ~11 ka. Instead, rainfall mainly controlled erosion in Central Chile. However, as mentioned above, precipitation records imply no major influence of rainfall on ^{10}Be/^{9}Be during that period.

The most likely cause of the observed changes in ^{10}Be/^{9}Be at our site across the Holocene is a change in ocean mixing with deep Pacific water containing higher ^{10}Be/^{9}Be ratios (Kusakabe et al., 1990). As mentioned above, an offshore ^{10}Be/^{9}Be core-top transect, studied at sites 700 km north of site J1004 (Wittmann et al., 2017) suggests that the ^{10}Be/^{9}Be ratio of continental shelf samples, like in our study site, is the mixture of two endmembers: a terrestrial endmember with low ^{10}Be/^{9}Be ratio ($\sim 2 \times 10^{-9}$) due to the high ^{9}Be supply from terrigenous rocks, and a PDW end-members with higher values ($\sim 1 \times 10^{-7}$) due to higher contribution of cosmogenic ^{10}Be to the ocean surface (Figure S4 in Supporting Information S1). Beryllium-9 is only sourced from terrigenous rocks, which may result in contrasting ^{9}Be concentrations in the coastal region and exported offshore. Thus, ^{10}Be/^{9}Be is likely to be high in open ocean and low in coastal margins. Considering the relationship between these two endmembers, we

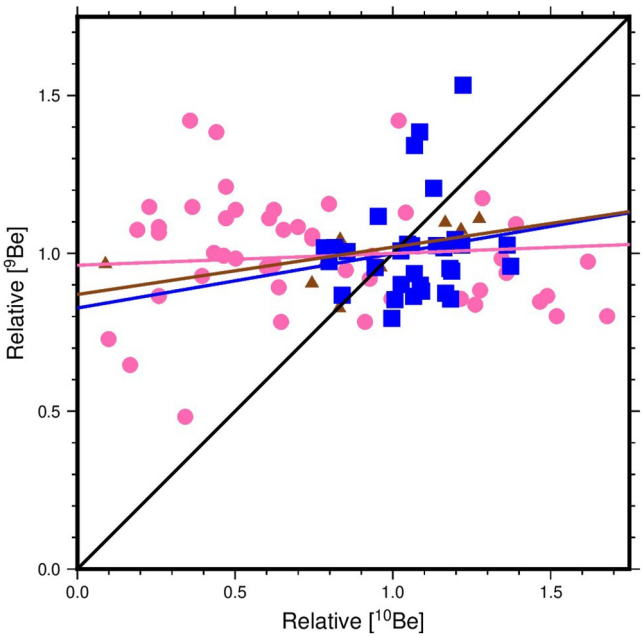

Figure 3. The relative (normalized by the average value) $[^{10}Be]_{reactive}$ and relative $[^{9}Be]_{reactive}$ plot of Site J1004 (blue squares), Site J1002 (Sproson et al., 2024; pink circles) and the present Chilean margin (Wittmann et al., 2017; brown triangles) with the 1:1 line and linear regression lines (blue: Site J1004; $y = 0.17x + 0.83$; $r^2 = 0.05$, pink: Site J1002; $y = 0.037x + 0.96$; $r^2 = 0.02$; brown: Wittmann et al., 2017; $y = 0.13x + 0.87$; $r^2 = 0.28$) for each data set.

interpret our $^{10}Be/^{9}Be$ record to primarily reflect progressive increase of the high $^{10}Be/^{9}Be$ PDW endmember to our site, relative to the terrestrial freshwater flux, driven by a southward shift of the SWWs throughout the Holocene (Figure 4b; Moreno et al., 2010, 2021). This interpretation is consistent with the conclusions of Jeromson et al. (2024, 2025). The reason for upwelling as a dominant factor for Be isotope signature in continental shelf margins, on the Antarctic and the Chilean margins, may be because of ~100 times difference in open ocean (PDW) and coastal $^{10}Be/^{9}Be$ values in both regions (Jeromson et al., 2024; Kusakabe et al., 1990). However, the non-monotonic changes in the generally increasing $^{10}Be/^{9}Be$ ratio between 5 and 4 ka suggest that other processes can have additional effects on the $^{10}Be/^{9}Be$ ratio and cannot simply be attributed to changes in the intrusion of PDW; however, the cause of this change is not the focus of this study.

Marine versus terrigenous mixing is also confirmed from the last deglacial period at Site J1002 by the relative ^{10}Be versus relative ^{9}Be plot. Both the relative ^{10}Be versus relative ^{9}Be relationship for the present Chilean margin and that of our data are parallel to the *X* axis in Figure 3, indicating that both fluctuations are caused by greater contribution of a secondary reactive layer derived from open marine conditions (Wittmann et al., 2017). Moreover, our relative ^{10}Be versus relative ^{9}Be plot is similar to that of Site J1002 (Sproson et al., 2024), which also implies that a similar mechanism drives Be concentrations along the Chilean margin. However, the main drivers of Be isotopes change at Site J1002 during the last glacial cycle and at J1007 during the Holocene are different. This is likely to be due to the absence of the PIS during the Holocene (Davies et al., 2020), allowing intrusion of PDW to become a dominant factor for Be ratio variation during interglacial periods. Conversely, during glacials and glacial terminations, the change in depositional setting related to the presence of an ice sheet on the continental shelf overwhelms the advective signal and dominates Be isotope variation (Sproson et al., 2024).

6.2. Increased Upwelling and Implications for Southern Ocean Productivity

Rejecting all other processes, we conclude the increase in $^{10}Be/^{9}Be$ ratio throughout the Holocene is likely to reflect an increase in Southern Ocean upwelling, which drove more PDW to our site. This conclusion is supported by additional lines of evidence of oceanic changes. The ~1°C cooling toward the late Holocene, indicated by the increase in the $\delta^{18}O$ record of planktonic foraminifera (*N. pachyderma*), is consistent with the alkenone SST record from the nearby ODP Site 1233 (41°S) showing continuous ~1°C cooling from ~12 ka to the present (Figure 4f; Kaiser et al., 2005). The $\delta^{18}O$ record of *N. pachyderma*, a surface-dwelling foraminifera that typically live at a depth consistent with the upper thermocline, is similar to the magnitude of $\delta^{18}O$ change in the benthic foraminifera *U. peregrina* at 1,100 m (Figures 4d and 4e). Therefore, we suggest that the cooling documented in the planktonic record was likely driven by an increasing contribution of cold PDW to this site and a shoaling of the thermocline. A lesser contribution of freshwater to the Chilean margin and shoaling of the thermocline would have been conducive to the strengthening of the upwelling in this region.

Studer et al. (2018), have documented a monotonic decrease in foraminiferal bound-$\delta^{15}N$ from the last deglaciation and throughout the late Holocene in sites around the Southern Ocean (Figure 4g; Martínez-García et al., 2014), attributed to a progressive decrease in biological pump efficiency, which likely enriched the preformed nutrients at the surface and therefore the ACC. Riechelson et al. (2024) have subsequently hypothesized that advection of the enriched preformed nutrients in the Southern Ocean (Studer et al., 2018) and their upwelling along the Chilean margin promoted high biogenic productivity. Indeed, the TOC accumulation rate at Site J1004 displayed similar increasing trends to $^{10}Be/^{9}Be$ across the Holocene, supporting the argument that upwelling induced an increase in productivity (Figure 2d; Riechelson et al., 2024). Near zero modern surface nitrate concentrations at the area of our site (WOCE Data Products Committee, 2002) is consistent with complete utilization of the upwelled nutrients, which led Riechelson et al. (2024) to suggest that the observed decrease in sediment

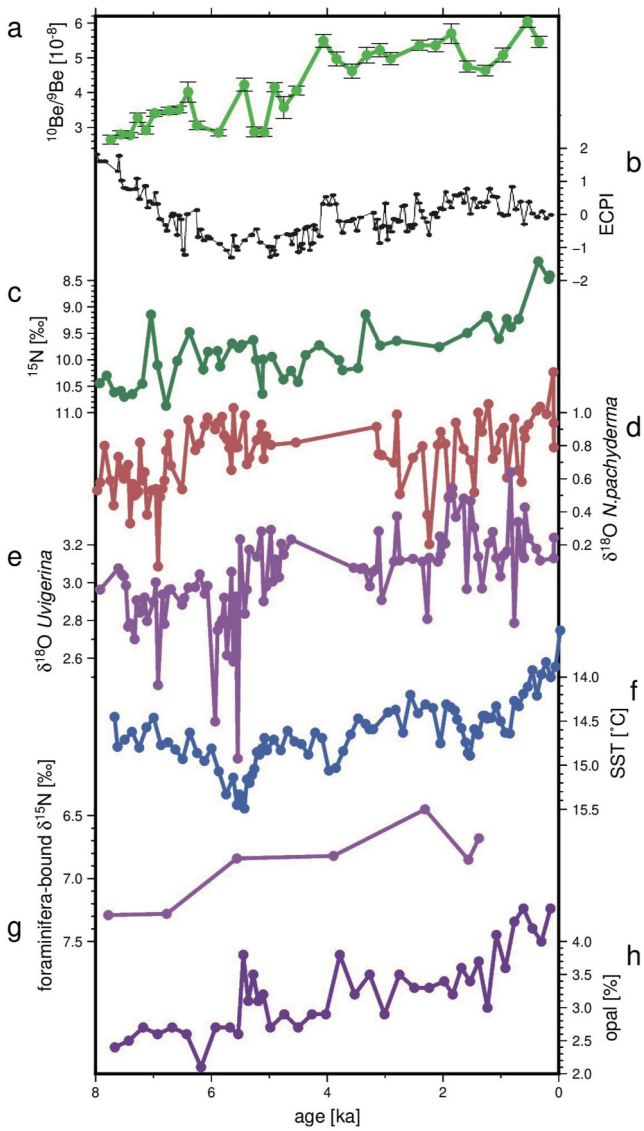

Figure 4. (a) Reactive ^{10}Be/^{9}Be ratios from offshore Chile (Site J1004A, 44°S) after 8 ka. (b) Normalized *Eucryphia* + *Caldcluvia*/podocarps index (ECPI) based on pollen assemblage at Lago Condorito negatively correlated with precipitation amount (41°S, Moreno et al., 2010). Panel (c) Same as (a) but for the δ^{15}N in the sediment (Riechelson et al., 2023). Panel (d) same as (a) but for the δ^{18}O of planktonic foraminifera *N. pachyderma*, (e) same as (a) but for the δ^{18}O of benthic foraminifera *U. peregrina*. (f) Alkenone sea surface temperature records from ODP1233 (41°S, Kaisar et al., 2005). (g) *G. bulloides* Foraminifera-bound δ^{15}N (Martínez-García et al., 2014). (h) Biogenic opal contents from Site GeoB3313-1 (41°S; Lamy et al., 2002).

δ^{15}N values throughout the Holocene at J1004 is also consistent with complete utilization of nitrate, and therefore the sediment δ^{15}N reflects an advected preformed signal from the Southern Ocean with variability inherited from the source region.

In the southern margin of Chile, increasing biogenic productivity throughout the Holocene is also confirmed by both biogenic opal content and total organic carbon content in core GeoB3313-1 located at 54°S (Figure 4h; Lamy et al., 2002). The increase in productivity throughout the Holocene at Site GeoB3313-1 is interpreted as the enhancement of the ACC (Lamy et al., 2002), which is consistent with increased upwelling at our site. As mentioned above, the enhanced upwelling trend throughout the Holocene in mid-latitude Chile is supported by the decrease in SST throughout the Holocene at Site ODP1233 (41°S; Figure 4f; De Pol-Holz et al., 2006; Lamy et al., 2007).

7. Conclusions

Here, we use Be isotopes (^{10}Be and ^{9}Be) analysis on marine sediments from core J1004A recovered from the Chilean margin to directly assess changes in upwelling along the Chilean margin during the Holocene previously hypothesized by Riechelson et al. (2023). The ^{10}Be/^{9}Be record from Site J1004 on the Chilean margin shows a general increasing trend throughout the Holocene. Based on the scatter plot between relative ^{10}Be and ^{9}Be, ^{10}Be/^{9}Be variability is mainly controlled by changes in mixing between fluvial and seawater sourced beryllium, which is consistent with modern setting on the Antarctic and Chilean margins (Jeromson et al., 2024, 2025; Wittmann et al., 2017). We suggest that the ^{10}Be/^{9}Be increase throughout the Holocene is most likely driven by enhanced upwelling and intrusion of PDW with higher ^{10}Be/^{9}Be compared with coastal water with lower ^{10}Be/^{9}Be. The enhancement of upwelling is consistent with an increase in biological productivity and low SSTs on the Chilean margin.

Based on δ^{15}N records from the Southern Ocean, it has been suggested that the progressive decrease in nutrients' utilization, due to increased upwelling from the last deglaciation throughout the Holocene, was the source for the late Holocene increase in atmospheric CO_2 (Studer et al., 2018). But it was further argued that export and consumption of upwelled nutrients along the Chilean margin might have reduced the contributions of the Southern Ocean as a marine CO_2 source to the Holocene increase in atmospheric CO_2 (Riechelson et al., 2024). While, the CO_2 record shows a decrease between 12 and 8 ka, followed by an increase starting ~6 ka, the marine records show generally monotonically increasing trends during the same time. This suggests that there were likely multiple processes acting at the same time both to increase and decrease atmospheric CO_2. Thus, the latter cannot be directly and linearly linked to the Southern Ocean changes upwelling but rather reflect the balance between these processes.

Conflict of Interest

The authors declare no conflicts of interest relevant to this study.

Data Availability Statement

Archiving data for replicating the results of this study are available at Pangaea (Nemoto et al., 2026).

Acknowledgments
We thank H. Matsuzaki (University of Tokyo) and members of MALT for their assistance with accelerator mass spectrometer measurements. We acknowledge Grants (20H00193 and 23KK0013 to Y.Y.; 18F18791 to Y.Y. and A.D.S.) from the Japan Society for the Promotion of Science and JST CREST (JPMJCR23J6 to Y.Y.). We acknowledge Grants from the National Science Foundation (OCE 1756241 to S.C.B. and Y.R.). We also express our gratitude to anonymous reviewers for their constructive comments that improved the quality of this manuscript.

References

Anderson, R. F., Ali, S., Bradtmiller, L. I., Nielsen, S. H. H., Fleisher, M. Q., Anderson, B. E., & Burckle, L. H. (2009). Wind-driven upwelling in the Southern Ocean and the Deglacial rise in atmospheric CO_2. *Science*, *323*(5920), 1443–1448. https://doi.org/10.1126/science.1167441

Behrens, B. C., Miyairi, Y., Sproson, A. D., Yamane, M., & Yokoyama, Y. (2019). Meltwater discharge during the Holocene from the Wilkes subglacial basin revealed by beryllium isotope analysis of marine sediments. *Journal of Quaternary Science*, *34*(8), 603–608. https://doi.org/10.1002/jqs.3148

Behrens, B. C., Yokoyama, Y., Miyairi, Y., Sproson, A. D., Yamane, M., Jimenez-Espejo, F. J., et al. (2022). Beryllium isotope variations recorded in the Adélie Basin, East Antarctica reflect Holocene changes in ice dynamics, productivity, and scavenging efficiency. *Quaternary Science Advances*, *7*, 100054. https://doi.org/10.1016/j.qsa.2022.100054

Bourles, D., Raisbeck, G. M., & Yiou, F. (1989). ^{10}Be and ^{9}Be in marine sediments and their potential for dating. *Geochimica et Cosmochimica Acta*, *53*(2), 443–452. https://doi.org/10.1016/0016-7037(89)90395-5

Bova, S., Rosenthal, Y., & Childress, L. (2019). Digging deeper with the JR100: Extending high resolution paleoclimate records from the Chilean Margin to the Eemian. https://doi.org/10.1002/2015PA002816

Chmeleff, J., von Blanckenburg, F., Kossert, K., & Jakob, D. (2010). Determination of the ^{10}Be half-life by multicollector ICP-MS and liquid scintillation counting. *Nuclear Instruments and Methods in Physics Research Section B: Beam Interactions with Materials and Atoms*, *268*(2), 192–199. https://doi.org/10.1016/j.nimb.2009.09.012

Davies, B. J., Darvill, C. M., Lovell, H., Bendle, J. M., Dowdeswell, J. A., Fabel, D., et al. (2020). The evolution of the Patagonian Ice Sheet from 35 ka to the present day (PATICE). *Earth-Science Reviews*, *204*, 103152. https://doi.org/10.1016/j.earscirev.2020.103152

De Pol-Holz, R., Ulloa, O., Dezileau, L., Kaiser, J., Lamy, F., & Hebbeln, D. (2006). Melting of the Patagonian Ice Sheet and Deglacial perturbations of the nitrogen cycle in the eastern South Pacific. *Geophysical Research Letters*, *33*(4). https://doi.org/10.1029/2005GL024477

Fyfe, J. C., & Saenko, O. A. (2006). Simulated changes in the extratropical Southern Hemisphere winds and currents. *Geophysical Research Letters*, *33*(6). https://doi.org/10.1029/2005GL025332

Garreaud, R., Lopez, P., Minvielle, M., & Rojas, M. (2013). Large-scale control on the Patagonian climate. *Journal of Climate*, *26*(1), 215–230. https://doi.org/10.1175/JCLI-D-12-00001.1

Gray, W. R., de Lavergne, C., Jnglin Wills, R. C., Menviel, L., Spence, P., Holzer, M., et al. (2023). Poleward shift in the Southern Hemisphere westerly winds synchronous with the Deglacial rise in CO_2. *Paleoceanography and Paleoclimatology*, *38*(7), e2023PA004666. https://doi.org/10.1029/2023PA004666

Jeromson, M. R., Fujioka, T., Fink, D., Simon, K., Post, A. L., Blaxell, M., et al. (2025). Beryllium-isotope signatures in ice sheet proximal marine sediments. *Chemical Geology*, *691*, 122912. https://doi.org/10.1016/j.chemgeo.2025.122912

Jeromson, M. R., Fujioka, T., Fink, D., Simon, K., Smith, J., Hillenbrand, C.-D., et al. (2024). Circumpolar deep water upwelling is a primary source of ^{10}Be in Antarctic continental shelf sediments. *Global and Planetary Change*, *236*, 104424. https://doi.org/10.1016/j.gloplacha.2024.104424

Kaiser, J., Lamy, F., & Hebbeln, D. (2005). A 70-kyr sea surface temperature record off Southern Chile (Ocean Drilling program site 1233). *Paleoceanography*, *20*(4). https://doi.org/10.1029/2005PA001146

Kohl, C. P., & Nishiizumi, K. (1992). Chemical isolation of quartz for measurement of in situ-produced cosmogenic nuclides. *Geochimica et Cosmochimica Acta*, *56*(9), 3583–3587. https://doi.org/10.1016/0016-7037(92)90401-4

Korte, M., Constable, C., Donadini, F., & Holme, R. (2011). Reconstructing the Holocene geomagnetic field. *Earth and Planetary Science Letters*, *312*(3–4), 497–505. https://doi.org/10.1016/j.epsl.2011.10.031

Kusakabe, M., Ku, T.-L., Southon, J. R., & Measures, C. I. (1990). Beryllium isotopes in the ocean. *Geochemical Journal*, *24*(4), 263–272. https://doi.org/10.2343/geochemj.24.263

Lal, D. (1991). Cosmic ray labeling of erosion surfaces: In situ nuclide production rates and erosion models. *Earth and Planetary Science Letters*, *104*(2–4), 424–439. https://doi.org/10.1016/0012-821X(91)90220-C

Lamy, F., Kaiser, J., Arz, H. W., Hebbeln, D., Ninnemann, U., Timm, O., et al. (2007). Modulation of the bipolar seesaw in the Southeast Pacific during termination 1. *Earth and Planetary Science Letters*, *259*(3–4), 400–413. https://doi.org/10.1016/j.epsl.2007.04.040

Lamy, F., Kilian, R., Arz, H. W., Francois, J.-P., Kaiser, J., Prange, M., & Steinke, T. (2010). Holocene changes in the position and intensity of the southern westerly wind belt. *Nature Geoscience*, *3*(10), 695–699. https://doi.org/10.1038/ngeo959

Lamy, F., Rühlemann, C., Hebbeln, D., & Wefer, G. (2002). High- and low-latitude climate control on the position of the southern Peru-Chile current during the Holocene. *Paleoceanography*, *17*(2), 16. https://doi.org/10.1029/2001PA000727

Lovenduski, N. S., Gruber, N., & Doney, S. C. (2008). Toward a mechanistic understanding of the decadal trends in the Southern Ocean carbon sink. *Global Biogeochemical Cycles*, *22*(3). https://doi.org/10.1029/2007GB003139

Martínez-García, A., Sigman, D. M., Ren, H., Anderson, R. F., Straub, M., Hodell, D. A., et al. (2014). Iron fertilization of the Subantarctic Ocean during the last ice age. *Science*, *343*(6177), 1347–1350. https://doi.org/10.1126/science.124684

Matsuzaki, H., Nakano, C., Tsuchiya, Y. S., Kato, K., Maejima, Y., Miyairi, Y., et al. (2007). Multi-nuclide AMS performances at MALT. *Nuclear Instruments and Methods in Physics Research Section B: Beam Interactions with Materials and Atoms*, *259*(1), 36–40. https://doi.org/10.1016/j.nimb.2007.01.145

McGlone, M. S., Wilmshurst, J. M., Richardson, S. J., Turney, C. S. M., & Wood, J. R. (2019). Temperature, wind, cloud, and the postglacial tree line history of sub-Antarctic Campbell Island. *Forests*, *10*(11), 998. https://doi.org/10.3390/f10110998

Menviel, L., & Spence, P. (2024). Southern Ocean circulation's impact on atmospheric CO_2 concentration. *Frontiers in Marine Science*, *10*, 1328534. https://doi.org/10.3389/fmars.2023.1328534

Moreno, P. I., Francois, J. P., Moy, C. M., & Villa-Martínez, R. (2010). Covariability of the Southern Westerlies and atmospheric CO_2 during the Holocene. *Geology*, *38*(8), 727–730. https://doi.org/10.1130/g30962.1

Moreno, P. I., Henríquez, W. I., Pesce, O. H., Henríquez, C. A., Fletcher, M. S., Garreaud, R. D., & Villa-Martínez, R. P. (2021). An early Holocene westerly minimum in the southern mid-latitudes. *Quaternary Science Reviews*, *251*, 106730. https://doi.org/10.1016/j.quascirev.2020.106730

Nemoto, K., Yokoyama, Y., Sproson, Miyairi, A. D. Y., Aze, T., Rosenthal, Y., et al. (2026). Beryllium isotope, major element and Foraminifera d^{18}O for sediment core J1004 [Dataset]. *PANGAEA*. https://doi.org/10.1594/PANGAEA.987374

Nishiizumi, K., Imamura, M., Caffee, M. W., Southon, J. R., Finkel, R. C., & McAninch, J. (2007). Absolute calibration of ^{10}Be AMS standards. *Nuclear Instruments and Methods in Physics Research Section B: Beam Interactions with Materials and Atoms*, *258*(2), 403–413. https://doi.org/10.1016/j.nimb.2007.01.297

Riechelson, H., Bova, S. C., Rosenthal, Y., Meyers, S., & Bu, K. (2023). Solar cycles forced Southern westerly wind migrations during the Holocene. *Geophysical Research Letters*, *50*(16), e2023GL104148. https://doi.org/10.1029/2023GL104148

Riechelson, H., Rosenthal, Y., Bova, S., & Robinson, R. S. (2024). Southern Ocean biological pump role in driving Holocene atmospheric CO_2: Reappraisal. *Geophysical Research Letters*, *51*(4), e2023GL105569. https://doi.org/10.1029/2023GL105569

Saunders, K. M., Roberts, S. J., Perren, B., Butz, C., Sime, L., Davies, S., et al. (2018). Holocene dynamics of the Southern Hemisphere westerly winds and possible links to CO_2 outgassing. *Nature Geoscience*, *11*(9), 650–655. https://doi.org/10.1038/s41561-018-0186-5

Siani, G., Michel, E., De Pol-Holz, R., DeVries, T., Lamy, F., Carel, M., et al. (2013). Carbon isotope records reveal precise timing of enhanced Southern Ocean upwelling during the last deglaciation. *Nature Communications*, *4*(1), 2758. https://doi.org/10.1038/ncomms3758

Sproson, A. D., Aze, T., Behrens, B., & Yokoyama, Y. (2021). Initial measurement of beryllium-9 using high-resolution inductively coupled plasma mass spectrometry allows for more precise applications of the beryllium isotope system within the Earth sciences. *Rapid Communications in Mass Spectrometry*, *35*(8), e9059. https://doi.org/10.1002/rcm.9059

Sproson, A. D., Takano, Y., Miyairi, Y., Aze, T., Matsuzaki, H., Ohkouchi, N., & Yokoyama, Y. (2021). Beryllium isotopes in sediments from Lake Maruwan Oike and Lake Skallen, east Antarctica, reveal substantial glacial discharge during the late Holocene. *Quaternary Science Reviews*, *256*, 106841. https://doi.org/10.1016/j.quascirev.2021.106841

Sproson, A. D., Yokoyama, Y., Miyairi, Y., Aze, T., Clementi, V. J., Riechelson, H., et al. (2024). Near-synchronous Northern Hemisphere and Patagonian Ice Sheet variation over the last glacial cycle. *Nature Geoscience*, *17*(5), 450–457. https://doi.org/10.1038/s41561-024-01436-y

Sproson, A. D., Yokoyama, Y., Miyairi, Y., Aze, T., & Totten, R. L. (2022). Holocene melting of the West Antarctic Ice Sheet driven by tropical Pacific warming. *Nature Communications*, *13*(1), 1–9. https://doi.org/10.1038/s41467-022-30076-2

Studer, A. S., Sigman, D. M., Martínez-García, A., Thöle, L. M., Michel, E., Jaccard, S. L., et al. (2018). Increased nutrient supply to the Southern Ocean during the Holocene and its implications for the pre-industrial atmospheric CO_2 rise. *Nature Geoscience*, *11*(10), 756–760. https://doi.org/10.1038/s41561-018-0191-8

Toggweiler, J. R., Russell, J. L., & Carson, S. R. (2006). Midlatitude westerlies, atmospheric CO_2, and climate change during the ice ages. *Paleoceanography*, *21*(2). https://doi.org/10.1029/2005PA001154

von Blanckenburg, F., Bouchez, J., Ibarra, D. E., & Maher, K. (2015). Stable runoff and weathering fluxes into the oceans over Quaternary climate cycles. *Nature Geoscience*, *8*(7), 538–542. https://doi.org/10.1038/ngeo2452

von Blanckenburg, F., Bouchez, J., & Wittmann, H. (2012). Earth surface erosion and weathering from the ^{10}Be (meteoric)/^{9}Be ratio. *Earth and Planetary Science Letters*, *351*, 295–305. https://doi.org/10.1016/j.epsl.2012.07.022

White, D. A., Fink, D., Post, A. L., Simon, K., Galton-Fenzi, B., Foster, S., et al. (2019). Beryllium isotope signatures of ice shelves and sub-ice Shelf circulation. *Earth and Planetary Science Letters*, *505*, 86–95. https://doi.org/10.1016/j.epsl.2018.10.004

Wittmann, H., von Blanckenburg, F., Bouchez, J., Dannhaus, N., Naumann, R., Christl, M., & Gaillardet, J. (2012). The dependence of meteoric ^{10}Be concentrations on particle size in Amazon River bed sediment and the extraction of reactive ^{10}Be/^{9}Be ratios. *Chemical Geology*, *318–319*, 126–138. https://doi.org/10.1016/j.chemgeo.2012.04.031

Wittmann, H., von Blanckenburg, F., Mohtadi, M., Christl, M., & Bernhardt, A. (2017). The competition between coastal trace metal fluxes and oceanic mixing from the ^{10}Be/^{9}Be ratio: Implications for sedimentary records. *Geophysical Research Letters*, *44*(16), 8443–8452. https://doi.org/10.1002/2017GL074259

WOCE Data Products Committee. (2002). NODC standard product: World ocean circulation experiment (WOCE) global data resource (GDR), versions 1-3, on CD-ROM and DVD [Dataset]. *NOAA National Centers for Environmental Information*. Retrieved from https://www.ncei.noaa.gov/archive/accession/NODC-WOCE-GDR

Yokoyama, Y., Anderson, J. B., Yamane, M., Simkins, L. M., Miyairi, Y., Yamazaki, T., et al. (2016). Widespread collapse of the Ross Ice Shelf during the late Holocene. *Proceedings of the National Academy of Sciences*, *113*(9), 2354–2359. https://doi.org/10.1073/pnas.1516908113

Yokoyama, Y., Maeda, Y., Okuno, J. I., Miyairi, Y., & Kosuge, T. (2016). Holocene Antarctic melting and lithospheric uplift history of the Southern Okinawa trough inferred from mid-to late-Holocene sea level in Iriomote Island, Ryukyu, Japan. *Quaternary International*, *397*, 342–348. https://doi.org/10.1016/j.quaint.2015.03.030

Yokoyama, Y., & Sproson, A. D. (2026). Beryllium isotopes in marine science: Understanding Ocean current and ice dynamics. *Annual Review of Marine Science*, *18*(1), 121–139. https://doi.org/10.1146/annurev-marine-040224-033226

Yokoyama, Y., Yamane, M., Nakamura, A., Miyairi, Y., Horiuchi, K., Aze, T., et al. (2019). In-situ and meteoric ^{10}Be and ^{26}Al measurements: Improved preparation and application at the University of Tokyo. *Nuclear Instruments and Methods in Physics Research Section B: Beam Interactions with Materials and Atoms*, *455*, 260–264. https://doi.org/10.1016/j.nimb.2019.01.026